



# Effect of Temperature on Macroscopic and Microscopic Properties of Sandstone From Qidong Coal Mine

Long-Chuan Deng<sup>1</sup> · Xiao-Zhao Li<sup>1,2</sup> · Ying-Chao Wang<sup>2</sup> · Yun Wu<sup>1,2</sup>  · Zhen Huang<sup>3</sup> · Chun-lu Jiang<sup>4</sup>

Received: 15 December 2020 / Accepted: 9 October 2021 / Published online: 23 October 2021  
© The Author(s), under exclusive licence to Springer-Verlag GmbH Austria, part of Springer Nature 2021

## Abstract

Heat from gas explosions affects the physical and mechanical properties of rock and reduces the stability of tunnels, such as in coal mines. This paper mainly studies the physical and mechanical properties of sandstone after heating and investigates the influences and mechanisms involved. Acoustic emission (AE) monitoring, X-ray diffraction (XRD), scanning electron microscopy (SEM) and polarized light microscopy are used to show that the uniaxial compressive strength (UCS) and peak strain of sandstone change significantly with temperature. In particular, the UCS decreases rapidly at 500~600 °C due to a transition from  $\alpha$ -quartz to  $\beta$ -quartz. The XRD analysis shows that the physical and mechanical properties of sandstone are affected by its mineral composition, as physical and chemical reactions of quartz, muscovite and kaolinite at high temperatures weaken the sandstone. The AE signals increase with temperature and correspond well with observed loading stages, as they reflect the spatiotemporal evolution in internal micro-cracks. The degree of crack opening is low at low temperatures, then cracks become connected with increasing temperature, further explaining the changes in mechanical properties. Polarized light microscopy shows that grain size and pore characteristics are related to mechanical strength; generally, higher strength is associated with smaller grains with a less even size distribution. In addition, thermal and mechanical damage were quantitatively characterized by deriving thermal, comprehensive and dynamic damage factors. The results provide a theoretical reference for mining engineering in high-temperature environments.

**Keywords** Thermal damage · Sandstone · High temperature · Physical and mechanical properties

## 1 Introduction

Sandstone is widely distributed in the earth's crust and has been used as an engineering material in the construction of buildings, monuments and other structures (Hajpal et al. 2002). Many famous buildings, such as the White House in the United States, and the Parliament building and Presidential Palace in India, are all built of sandstone (Dorn et al. 2003; Fitzner et al. 2003; Gautam et al. 2016a, b). Sandstone is often encountered during deep underground engineering activities such as tunnelling, geothermal exploitation and oil drilling, and especially in coal mines, where the roof and floor of the coal seams are mostly sandstone (Zhu et al. 2016; Zhang et al. 2010). Moreover, tunnels and monuments are at risk of fire, while coal mines are also at risk of gas explosions due to high temperatures, which can reach more than 1000 °C at depth, it affects the stability of surrounding rock. (Gautam et al. 2016a, b; Rong et al. 2018; Sirdesai et al. 2018; Verma et al. 2013). For example, the stability of the rock structure is affected by stress distribution, water

---

✉ Xiao-Zhao Li  
lixz@nju.edu.cn

✉ Yun Wu  
wy1562254170@163.com

<sup>1</sup> School of Earth Sciences and Engineering,  
Nanjing University, Nanjing, Jiangsu 210046,  
People's Republic of China

<sup>2</sup> State Key Laboratory for Geomechanics and Deep  
Underground Engineering, China University  
of Mining and Technology, Xuzhou, Jiangsu 221116,  
People's Republic of China

<sup>3</sup> School of Resources and Environment Engineering,  
Jiangxi University of Science and Technology, Ganzhou,  
Jiangxi 341000, People's Republic of China

<sup>4</sup> School of Resources and Environmental Engineering, Anhui  
University, Hefei 230601, People's Republic of China

state, apparent colour, and rock mineral phase transitions, (Fuenkajorn et al. 2012; Zhu et al. 2018). There is a risk of gas explosion deep in the Qidong coal seam according to the survey data. Therefore, it is necessary to fully understand the physical and mechanical properties of sandstone subjected to high temperatures and evaluate its thermal stability so as to provide a reference for its effective use.

So far, research on the physical and mechanical properties of sandstone subjected to high temperatures has mainly focused on uniaxial compressive strength, indirect tensile strength, elastic modulus and P-wave velocity, mass loss, porosity, permeability, Poisson's ratio, peak strain, crack density and fracture surface roughness and glossiness. (Feng et al. 2020; Malkowski et al. 2012; Wu et al. 2005, 2018; Wang et al. 2017; Wu et al. 2020, 2021; Yavuz et al. 2010; Yin et al. 2018; Zhang et al. 2020a; Zeng et al. 2018; Zhao et al. 2019a; Zhang et al. 2017a). A series of studies have shown that the physical and mechanical properties of sandstone change after high-temperature treatment. For example, Li et al. (2020a) analysed the pore structure and mechanical characteristics of sandstone after treatment at different temperatures. They found that the size and number of pores are related to the number of cracks. Yang et al. (2017) found that the cohesion and internal friction angle increase at low-to-middle temperatures, while the opposite trend occurs at high temperatures, and permeability also changes significantly. Zhang et al. (2021) found from a systematic analysis of a large amount of data that there are three changing patterns of uniaxial compressive strength and P-wave velocity after heating of sandstones, and that the variation of uniaxial compressive strength is mainly due to microstructure and quartz content. The inconsistency between P-wave velocity and uniaxial compressive strength is mainly related to water content, quartz content and specific minerals. The sandstone is subject to thermal stress at high temperatures and causes expansion of the mineral, which in turn changes the physical and mechanical properties and internal structure, creating microscopic defects (Tian et al. 2016). Yu et al (2015) carried out mechanical tests on heat-treated red sandstone and found that the colour, strength and permeability were altered. Many references related to this topic have also been conducted (Huang et al. 2021a; Kong et al. 2016; Sun et al. 2016; Shen et al. 2018; Yang et al. 2014). The mechanical properties of the sandstone under different heat treatment conditions are summarized in Table 1.

Currently, the study of rock thermal damage is mainly divided into macro-scale (mechanical parameters, apparent morphology, failure modes) and micro-scale effects (mineral analysis, micro-structures) (Liu et al. 2020). Research methods mainly include mechanical tests, physical tests, X-ray diffraction, SEM, thin-section analysis, computed tomography (CT) technology, digital imaging and AE techniques (Feng et al. 2018 Huang et al. 2021b; Kong et al. 2017;

Lu et al. 2017; Li et al. 2020a; Mahanta et al. 2020; Sun et al. 2017; Zhang et al. 2017b, 2017c). For example, Zhang et al. (2020b) studied the influence of mineral content and composition on the thermal damage of limestone. SEM, CT technology and thin-section analysis are effective ways to analyse the evolution of cracks in rocks after heating and to reveal the characteristics of rock mineral grains (Zhang et al. 2021). Nara et al. (2011) studied the crack patterns of sandstone after heating using thin section analysis. AE technology can monitor changes in internal structure during the dynamic loading of rocks, and reflects the development of internal cracks and transient events caused by unstable states (Zhao et al. 2020). Zhao et al. (2019b) investigated the differences in the characteristics of AE *b* values during deformation and damage of inclusions in three stress paths and concluded that the AE *b* values are closely related to the loading path, with large differences in the variation pattern of *b* values under loading and unloading paths. Han et al. (2020) analysed the AE signals of sandstone after water-cooling based on uniaxial compression tests and showed that the damage of the specimen lagged behind the aggregation of the AE signals.

As can be seen from the above analysis, the physical and mechanical properties of the sandstone after heat treatment are currently being studied more frequently. This paper focuses on the thermal damage mechanism of the sandstone, and defines three different damage variables, namely thermal damage variable, compressive damage variable and dynamic damage variable based on various physical and mechanical parameters measured by uniaxial compressive strength tests and AE parameters, and investigates the static and dynamic properties of thermal damage of the sandstone. The thermal damage mechanism of the sandstone was also revealed by means of AE, SEM, polarized light microscopy, XRD and literature comparisons, and the damage degree after heat treatment of the sandstone was investigated qualitatively as well as semi-quantitatively. This work has important application value for mining engineering and provides a theoretical reference on the stability of the sandstone after high temperature.

## 2 Experimental Samples and Methods

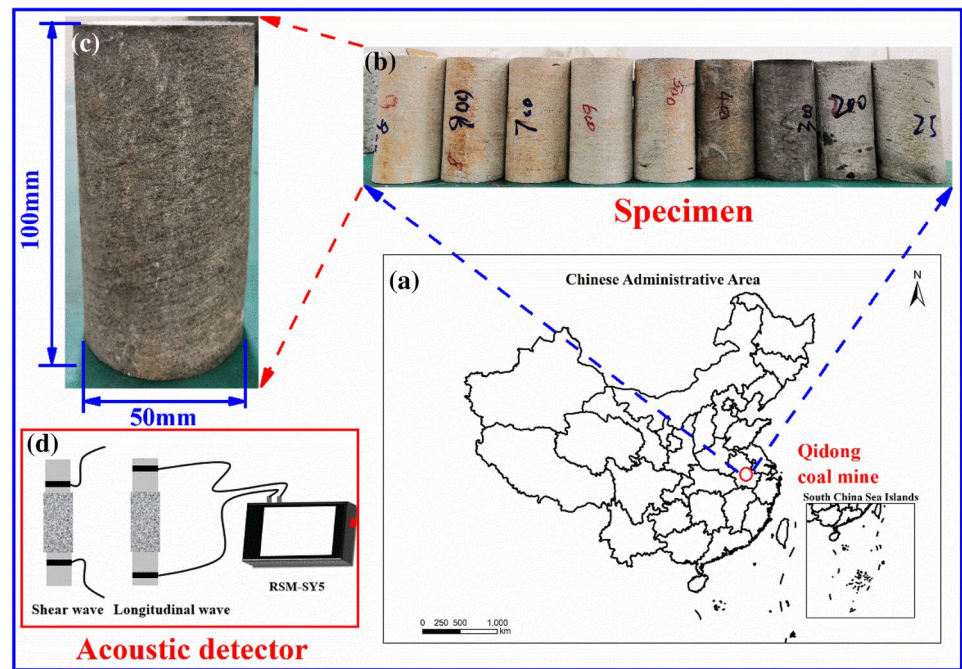
### 2.1 Collection and Preparation of Sandstone

Sandstone samples were collected from depths of 420–510 m in the Qidong coal mine, Anhui Province, China Fig. 1(a). All samples were processed into 50 × 100mm cylinders to meet the requirements of the ISRM (Fairhurst et al., 1999). The P-wave velocities of the samples were measured using an acoustic detector (RSM-SY5 (T)). The average P-wave velocity and average

**Table 1** Some literature about mechanical properties of different sandstones in different conditions

Rock	Sample size	Temperature range (°C)	Heating path	Loading rate	Parameters	References
Sandstone from Pingshuo coalmine	φ50mm × 100 mm	20, 200, 400, 500, 600, 700, 800	Heating at 20 °C/min for 2 h	Confining pressure: 0.08 MPa/s	Permeability, Volume, Peak strength, Young's modulus, Thermal stress	Ding et al. (2016)
Sandstone from Rizhao city	φ50mm × 100 mm	25, 250, 500, 750, 1000	Heating at 5 °C/min for 2 h	Brazilian tensile tests: 0.02 mm/min Triaxial compression tests: hydrostatic pressures at a rate of 5 MPa/min, loading pressure at a rate of 0.02 mm/min	Tensile strength, Fracture toughness, Young's modulus, Poisson's ratio,	Yang et al. (2017)
Coarse sandstone	φ50mm × 100 mm	25 ~ 900	Heating at 10 °C/min for 4 h	Displacement control: 0.005 mm/s	p-wave velocity, Peak strain, secant modulus	Su et al. (2008)
Red sandstone	Thickness: 25 ~ 50mm Ratio of thickness to radical dimension: 0.5 ~ 1.0	200, 400, 600, 80	Heating at 20/min for 50 min	Displacement control: 0.0025/s	Tensile strength, failure pattern,	Su et al. (2015)
Sandstone from Jiaozuo	φ50mm × 100 mm	20, 100, 150, 200, 400, 600, 800, 1000, 1200	Heating at 5 °C/min for 2 h	Displacement control	Apparent shape, Compressive strength, Peak strain, Elastic modulus, Poisson's ratio,	Wu et al. (2007)
Coarse sandstone	φ50mm × 100 mm	100 ~ 900	Heating at 30 °C/min for 5 h	/	Density, P-wave velocity, Tensile strength,	Zhao et al. (2010)

**Fig. 1** The location and physical map of sandstone specimens



shear velocity were 4385 m/s and 2369 m/s, respectively Fig. 1(d). The average density and uniaxial compression strength (UCS) at room temperature were  $2.67 \text{ g/cm}^3$  and 95.2 MPa, respectively. The sandstone is bluish-grey with a compact structure and no obvious surface cracks. The experiment scheme is shown in Table 2.

## 2.2 Thermal Treatment and Cooling Method

After the sandstone was processed into standard cylindrical samples, those with similar P-wave velocities were grouped for testing to ensure testing accuracy. They were dried in an oven at  $105 \text{ }^\circ\text{C}$  to reduce the negative influence of variable water contents. Then, 20 samples were divided into 10 groups; each group of samples was placed in a muffle furnace (TNX-1400) and heated to one of ten temperatures: 200, 300, 400, 500, 600, 700, 800, 900 or  $1000 \text{ }^\circ\text{C}$ . A heating rate of  $8 \text{ }^\circ\text{C}/\text{min}$  was used to avoid causing thermal shock to the samples. After each set of samples reached the target temperature, maintained for 2 h to ensure even heating, then samples were cooled to room temperature in the furnace (Fig. 2).

## 2.3 Uniaxial Compressive Tests and Acoustic Emission Tests

After the specimen is heated, the P-wave velocities were measured to preliminarily reflect the damage degree of sandstone. For the uniaxial compression test, a microcomputer-controlled electro-hydraulic servo rock triaxial testing machine was used (TAW-2000; Fig. 3). The displacement control method was adopted in the test and a loading rate of  $0.1 \text{ mm}/\text{min}$  was used. Radial and axial strain gauges were used to measure the axial and radial deformations in the process of rock compression.

The AE instrument used in this work was an AMSY-6 (Fig. 3). This system is mainly composed of an AE probe, AE pre-amplifier, data acquisition system and computer system. The AE monitoring parameters used in the uniaxial compressive tests were a threshold value = 38 dB and acquisition frequency = 5 MHz, with AE signal detection conducted through a single channel. The AE probe was fixed in an appropriate position on the rock surface with adhesive tape. To better monitor the signals released during the rock fracture process, the probe and rock surface foundation were daubed with vaseline.

**Table 2** Experiment scheme

Temperature level ( $^\circ\text{C}$ )	Heating rate ( $^\circ\text{C}/\text{min}$ )	Physical and Mechanical properties	Microscopic properties
25, 200, 300, 400, 500, 600, 700, 800, 900, 1000	Heating at $8 \text{ }^\circ\text{C}/\text{min}$ for 2 h	Uniaxial compressive strength P-wave velocity, Peak strain, Acoustic emission, Damage degree	SEM, Polarizing microscope, XRD

**Fig. 2** Heating equipment and heating path

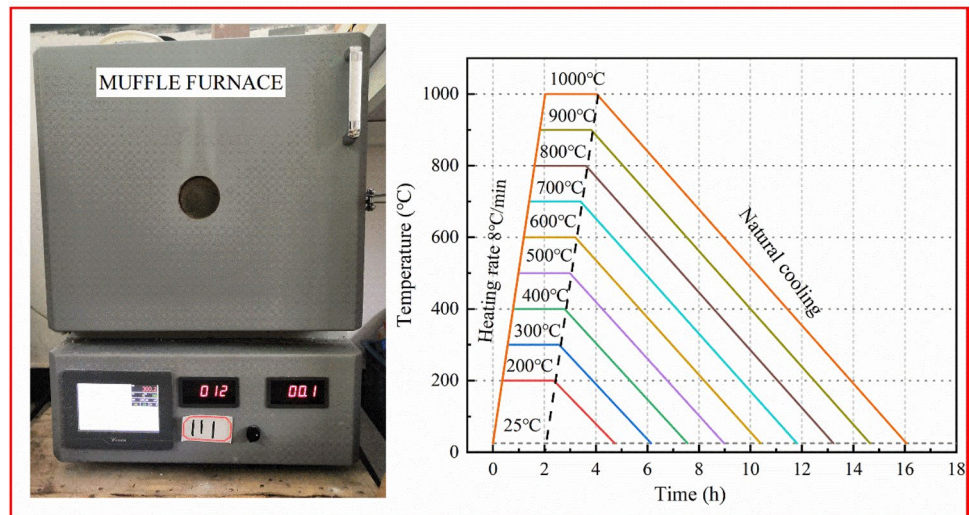
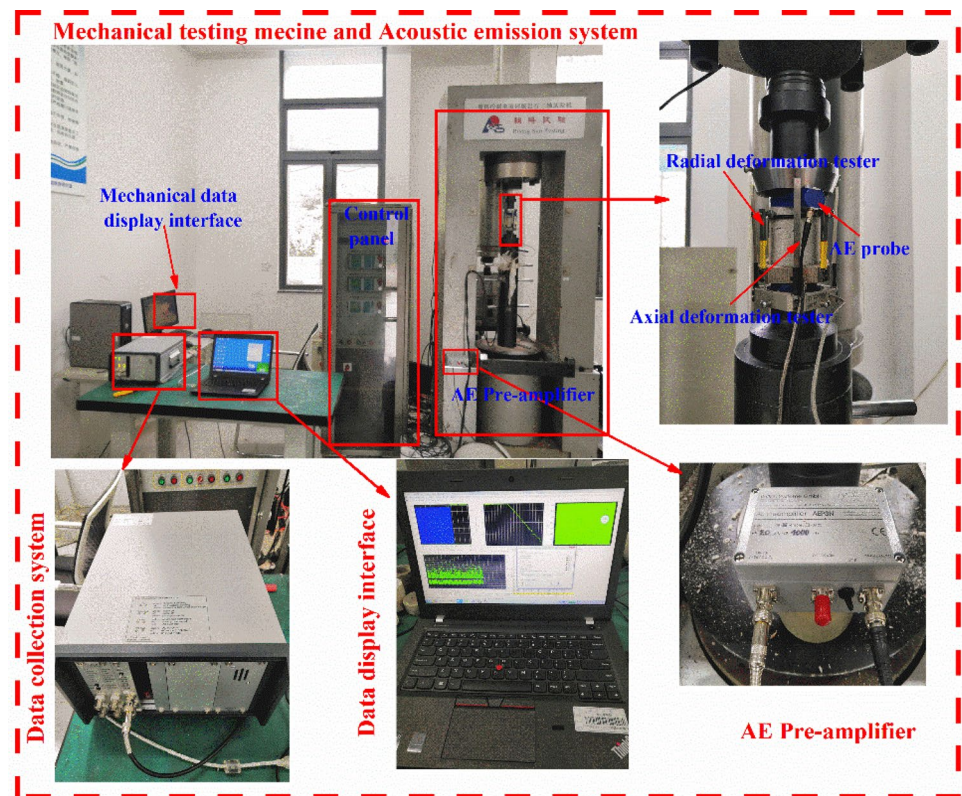


**Fig. 3** Uniaxial compressive test equipment and AE monitoring equipment



**2.4 Mineralogy**

Physical processes and chemical reactions (such as dehydration, decomposition, mineral phase transformation, sintering, dehydroxylation) at different temperatures have great impacts on rocks, essentially changing their mineral composition (Zhang et al. 2020b). Therefore, research on changes in rock mineral composition is vital to understand the physical and mechanical properties. The XRD tests found that,

in its natural state, the mineral composition of sandstone mainly includes 93% of quartz, 4.2% of muscovite and 2.8% of feldspar and kaolinite. The quartz content was > 90%, indicating that the samples were of quartz sandstone.

**2.5 SEM and Polarized Light Microscope**

The internal structure of the rock is closely related to physical and mechanical properties. SEM and thin-section

analysis were used to observe the effects of temperature on the mechanical properties of sandstone treated at different temperatures. Thin-section analysis is the process of making thin slices of samples and observing them under a polarized-light microscope, which has plane-polarized and crossed-polarized light modes. This method can be used to identify minerals and their morphology and crack distribution. SEM can observe the morphology of cracks at a finer scale than thin-section analysis.

### 3 Results and Discussion

#### 3.1 Effect of Temperature on Mechanical Properties of Sandstone

##### 3.1.1 Variation of Stress–Strain

Figure 4 shows the stress–strain curves of the sandstone heated to different temperatures. It can be seen from the figure that the stress–strain curves of natural and heat-treated sandstone can be roughly divided into four stages: (I) crack compaction, (II) elastic, (III) failure and (IV) post-peak stages. During each of these four stages, the internal structure of the rock undergoes the development of initial crack compaction, new crack formation, crack extension and crack penetration, showing that rock damage is a cumulative process. After the failure of the sample, the stress does not suddenly decline precipitously but gradually declines for several seconds, followed by a linear decline. However, for some rocks, the samples still had a certain capacity to resist external deformation after failure, which is called the residual compressive strength. The transition for stress–strain curve is 500 °C in Fig. 4, for stage I, it can be clearly seen

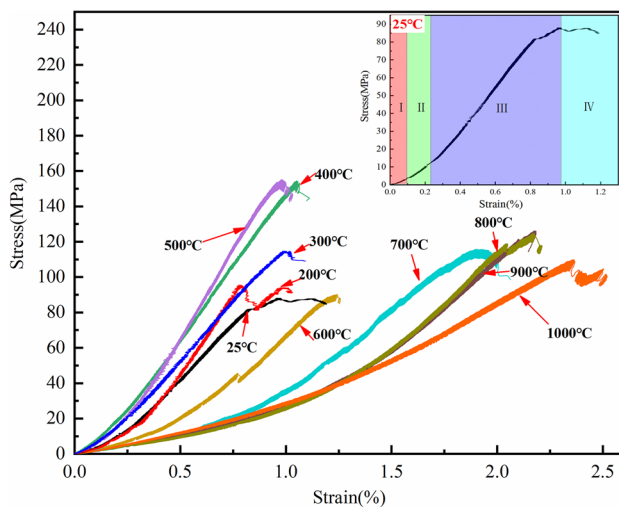


Fig. 4 Stress–strain curves of sandstone at different temperatures

from the figure that the stage duration gradually becomes shorter at 25 °C–500 °C and much longer at 600 °C–1000 °C than other temperature stages, trends in the other stages are similar to those in stage I. A similar phenomenon occurred in parts of the literature, with the sandstone stress–strain curves measured by Sirdesai et al (2017); Li et al (2020b), also turns around 500 °C. However, some literature (Li et al. 2020c) suggests that the stress–strain curve for sandstone turns at 400 °C or other temperatures, which is mainly related to the pore properties of the sandstone. In general, the mechanical properties of sandstones are strengthened at low temperatures, but weakened with increasing temperatures and undergo a transformation from brittle to ductile.

##### 3.1.2 UCS and Peak Strain

It can be seen from Fig. 5 that the variation in the average uniaxial compressive strength of sandstone with temperature can be divided into four stages: a rapid growth stage, a sharp decreasing stage, a modest growth stage and a general decreasing stage. At 25 °C–500 °C, the average uniaxial compressive strength of sandstone rises rapidly with increasing temperature, from 95 MPa at room temperature to 151 MPa at 500 °C, an appropriately 58.94% rise. Meanwhile, the peak strain of the sandstone in this temperature range gradually becomes smaller. Some of the original pores and fractures become closer under the action of thermal stress at 500 °C, resulting in the peak strain of the sandstone reaching a minimum and the uniaxial compressive strength reaching a maximum. When heated to 600 °C, the uniaxial compressive strength of the sandstone decreases sharply because of the transition of  $\alpha$ -quartz to  $\beta$ -quartz (Xi et al. 1994). The internal structure of the sandstone suffers severe damage and the degree of opening

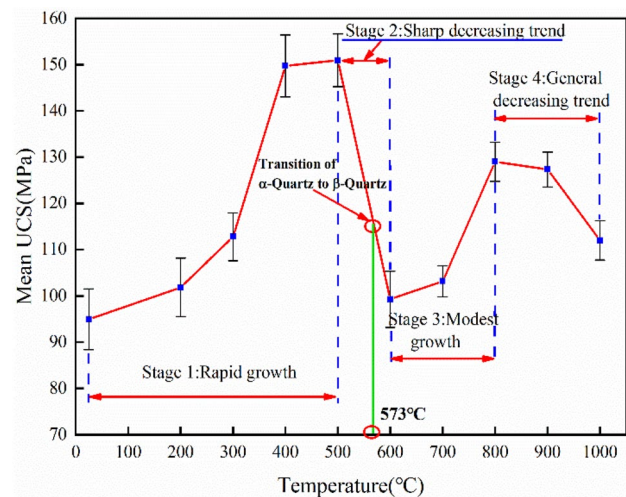


Fig. 5 Variation of mean UCS of sandstone with temperature

among cracks gradually increases, leading to a significant decrease in uniaxial compressive strength and an increase in the peak strain. At 600–800 °C, the uniaxial compressive strength increases slowly and the peak strain increases significantly due to the melting of minerals and grain size (as mentioned in Sect. 3.4.3). Above 800 °C, the samples suffered serious damage due to heat, so that the uniaxial compressive strength decreased while the peak strain continued to increase (Fig. 6).

## 3.2 Acoustic Emissions

### 3.2.1 Characteristics of AE Counts and Accumulated AE Counts

As mentioned before (Sect. 3.1.1), the stress–strain curves can be divided into four stages (compression, elastic, failure, post-peak). The AE in the four stages have different laws and reflects the damage characteristics of the rock. The AE signal corresponds well to the stress development characteristics of the rock as can be seen in Fig. 7. The AE ringing counts are more active during the crack compression stage and are weak when entering the plastic deformation stage. As new cracks form, expand and penetrate within the rock, the AE ringing counts begin to get progressively larger, and are greatest when the rock is broken. The cumulative AE ringing counts first increase at a rapid rate, then develop in a near-horizontal line, and finally increase at a greater rate to the maximum. Occasional small steps also occur during the change in the cumulative AE ringing count as can be seen in Fig. 7(d, e) indicating that energy is being released from the rock. The sample at room temperature has weak AE signals before failure (Fig. 7a). The cumulative AE ringing count curve develops in an almost horizontal straight line

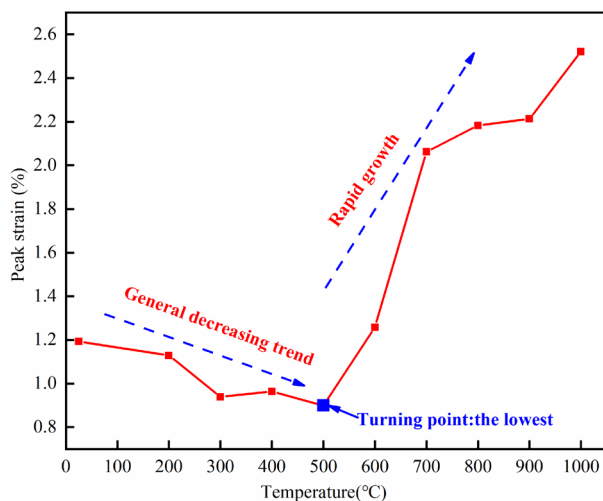


Fig. 6 Variation of peak strain of sandstone with temperature

and a large amount of AE signals cannot be detected until the samples are destroyed, which is associated with changes in the internal structure of the rock and brittle-plastic alterations. With increases in temperature, AE signals are more intense and active during the whole loading process. This is manifested as AE signals increase in the initial loading stage increases with temperature, and obvious signal peaks also appear in the elastic and failure stages. In short, AE signals are released in each stage with increases in temperature. It can be observed from the figure that damage to the sample is incremental, especially by observing the AE signal characteristics near the point of destruction. Therefore, an early warning of sandstone destruction can be obtained by observing the variation in the AE ringing counts. This can provide a timely disaster warning for underground engineering projects in theory.

### 3.2.2 Characteristics of AE $b$ Values Throughout Loading

The  $b$  value is derived from the relationship between earthquake frequency and magnitude, and was proposed by Icher et al. (1944). Rock failure is similar to the mechanism of earthquake, from which the concept of the  $b$ -value was derived and applied to acoustic emission technology (Liu et al. 2017). The  $b$ -value is calculated by the following formula (Fu et al. 2016):

$$\lg N = a - b \left( \frac{A_{dB}}{20} \right) \quad (1)$$

where  $A_{dB}$  is the AE amplitude, which is usually set by itself according to the data situation.  $N$  is an equal number of AE events with amplitudes  $> A_{dB}$  selected in a specific time window to determine the  $b$ -value,  $a$  is a constant, and  $b$  is the parameter we need to obtain. This paper adopts a scanning algorithm for this calculation. To ensure the feasibility of calculating the AE  $b$  value, 5000 events were taken as a fixed time window for calculating the  $b$ -values based on AE data.

Increases in  $b$  value indicates that the development of rock cracks is dominated by small-scale cracks, while decreases mean that the rock cracks tend to develop towards large-scale cracks (Liu et al. 2019). By analysing the variation of  $b$  value with temperature during the loading process (Fig. 7), it can be seen that the  $b$ -value of sandstone showed a dynamic change during the uniaxial compression test. It can be seen from Fig. 7(a) that the  $b$ -value increased slightly at the initial loading stage, indicating that the sandstone mainly developed small-scale cracks. Subsequently, large-scale cracks gradually developed inside the sandstone due to increases in axial stress, and the  $b$ -value kept decreasing and reached a minimum when the sample was about to be destroyed. Within the temperature range of 200–400 °C, the  $b$  value variation was the same as at room temperature;

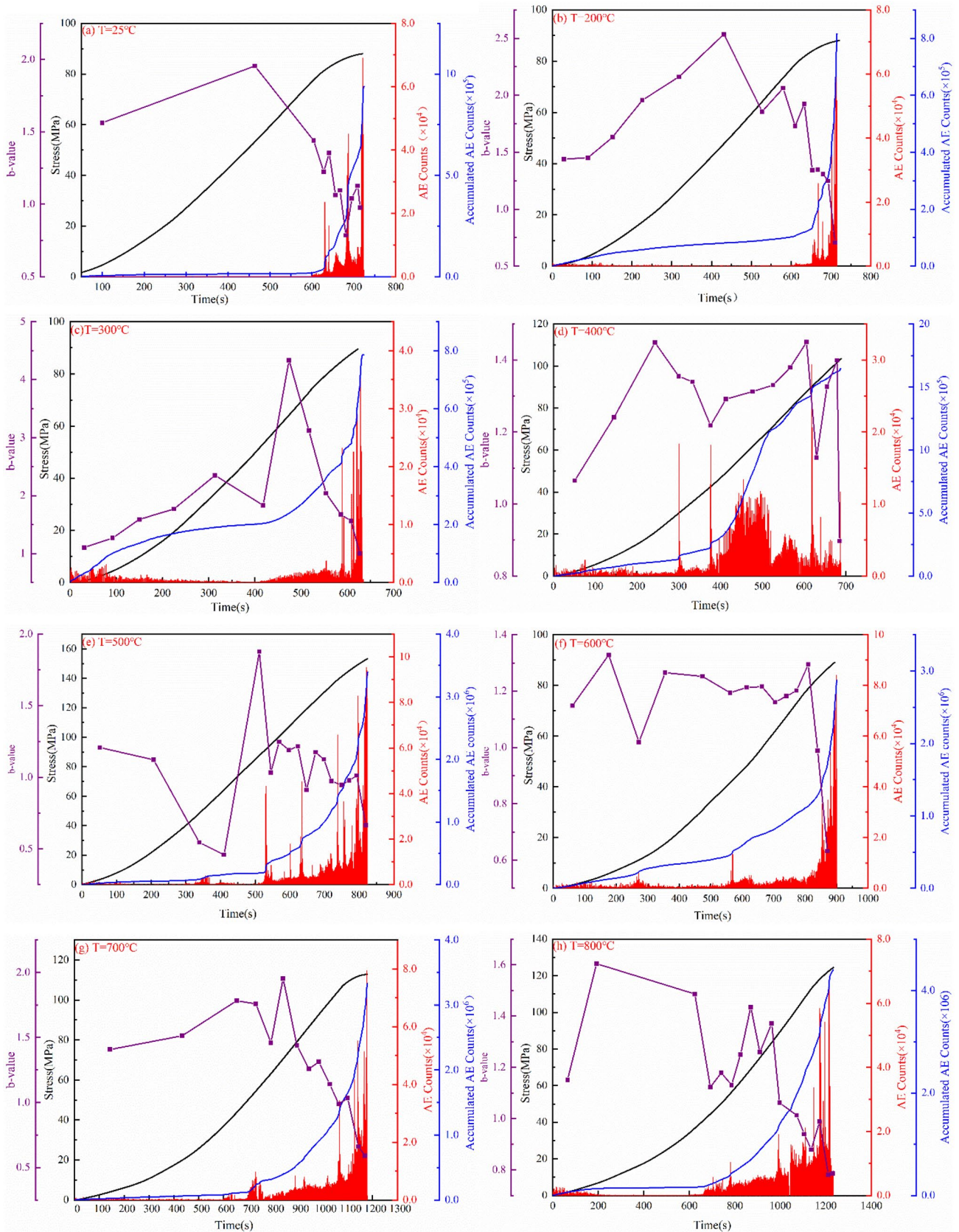


**Fig. 7** The curves of AE characteristics in the whole procedure at different temperatures



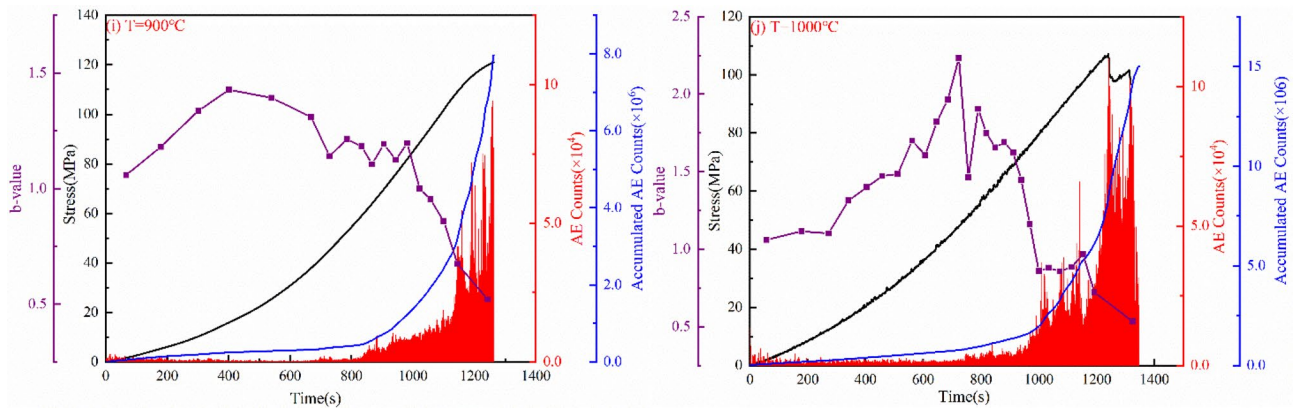


Fig. 7 (continued)

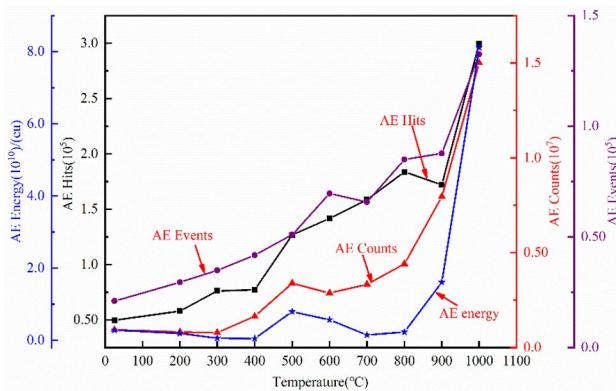


Fig. 8 Variation of AE parameters with temperature

that is, the *b* value increased at the initial loading stage and decreased in the later stage. At 500 °C and 600 °C, the *b* value first decreased and then increased with increases in axial stress, and finally dropped sharply when the sample was about to be destroyed. The *b* value still fluctuated above 600 °C but the overall trend was still one of increasing first and then decreasing. This is also in line with the characteristics of crack development during the sample failure process. That is, cracks developed from small-scale to large-scale as the loading process continued.

### 3.2.3 Variation of AE Parameters with Temperature

In addition to the AE count, AE parameters include the AE hit, AE event, AE energy, AE amplitude and others. Figure 8 shows the variations of four AE parameters with temperature. The following conclusions can be roughly made by analysing these relationships: (1) AE hit, AE event, AE energy and AE count all show increases with temperature. (2) These four trends can be roughly divided into two stages occurring at 25–500 °C and 500–1000 °C. (3) In the first

stage, the AE parameters are generally slowly increasing, with AE events and AE hits increasing slowly in a straight line and AE counts and AE energy increasing slowly in a fluctuation. (4) After 500 °C, the AE parameters increase rapidly with temperature, especially after 900–1000 °C. The four parameters show increases of nearly 90°, among which the AE energy increases about 4.5-fold between 900 °C and 1000 °C. (5) The trends in these AE parameters correspond well with the trends in sandstone’s peak stress (Fig. 5), peak strain (Fig. 6), providing information on the influence of temperature on sandstone. (6) The time-series characteristics of these AE parameters provide a detailed reflection of damage to the rock structure. An active AE signal means that the rock structure is experiencing great changes; therefore, the trends in AE parameters are a better indication of rock damage.

The crack initiation occurs at about 40% of the peak stress and unstable crack development occurs at about 80% of the peak stress as mentioned in Cai et al. (2004). Therefore, the relationship between the cumulative ringing counts and temperature at these two stress levels was analysed, as shown in Fig. 9. It can be seen from Fig. 9 that the cumulative ringing counts at all temperatures are almost within the same range, only increasing slightly with temperature when the stress reaches 40% of the peak stress. The curve increases rapidly with temperature when the stress reaches 80% of the peak stress, and the growth rate of the curve reaches its maximum after 700 °C. The difference between the two curves also increases as the heating temperature increases. By analysing these trends, it is evident that the cracks produced by sandstone at different temperatures are few and similar in the initial loading stage, while internal cracks leading to failure are mainly produced in the late loading stage. It can be concluded that the numbers of cracks induced at different temperatures do not differ greatly and cracks are mainly generated gradually under the action of axial stress. Since the temperature has weakened the sample, the higher the

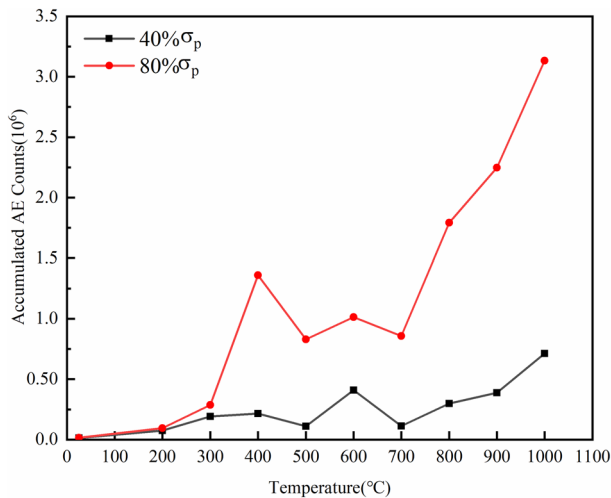


**Fig. 9** Variation of accumulated AE counts with the temperature at the point of 40% or 80% of peak stress

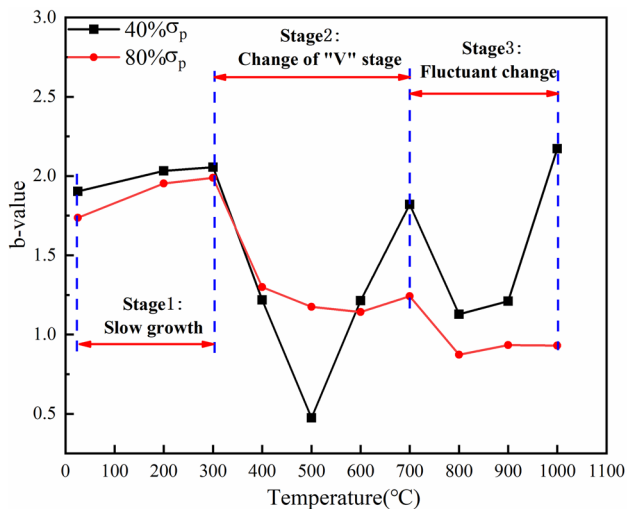


**Fig. 10** The variation of b-value with the temperature at the point of 40% or 80% of peak stress

heating temperature, the more likely cracks are to be generated by axial stress.

Temperature has a great impact on crack size; the size of the cracks formed can be quantified by analysing the variation in the AE b-value with temperature. Figure 10 shows this variation at two key points: 40% and 80% of the peak stress. Accordingly, the relationship can be divided into three stages based on the trends. Both curves show a slow increase in the first stage, and then the AE b-value has a characteristic “V” shape in the second stage with a minimum at 500 °C. The AE b-value then fluctuates in the third stage. It can be seen that, at a high-stress level, the AE b-value is generally lower than at a low-stress level,

indicating that the crack gradually develops to a large scale as loading continues. The higher the temperature, the lower the AE b-value at the two stress levels, showing that the temperature causes gradual development of the crack to a large scale, further aggravating damage to the sample.

### 3.3 Damage Degree

Damage caused by temperature and external loads are referred to the thermal and mechanical damage, respectively. Several damage variables were defined to quantify these two damage types and their degrees in sandstone. In addition, to describe deformation and crack development in sandstone during the failure process, a time-series of damage characteristics during the failure process was studied.

#### 3.3.1 Thermal Damage Degree

The characteristics of P-wave velocity can quantitatively reflect thermal damage to the rock. Thermal damage to rock is generally irreversible. Based on the elastic theory, the relationship between the mechanical parameters of rock and the P-wave velocity can be described by Eqs. (2) and (3) (Ferrero et al. 2009). A damage variable can be used to describe the specific conditions of deformation and fracture in sandstone. The damage variable of the rock after heat treatment can be calculated by Eq. (4) (Liu et al. 2000).

$$E = \rho V_p^2 \frac{(1 + \mu)(1 - 2\mu)}{1 - \mu} \quad (2)$$

$$\mu = \frac{\left(\frac{V_p}{V_s}\right)^2 - 2}{2\left(\frac{V_p}{V_s}\right)^2 - 1} \quad (3)$$

$$D_T = 1 - \frac{E_T}{E_0} \quad (4)$$

where  $E$  is the dynamic elastic modulus,  $\rho$  is the volume density of the rock,  $V_p$  is the P-wave velocity,  $v_s$  is the shear wave velocity,  $\mu$  is the dynamic Poisson's ratio of the rock,  $E_T$  is the elastic modulus at temperature  $T$ ,  $E_0$  is the elastic modulus at room temperature, and  $D_T$  is the thermal damage factor. The relationship between the thermal damage factor and temperature is plotted in Fig. 11. It shows that the thermal damage factor; that is, temperature-induced defects in the internal structure of sandstone generally increase linearly with temperature.

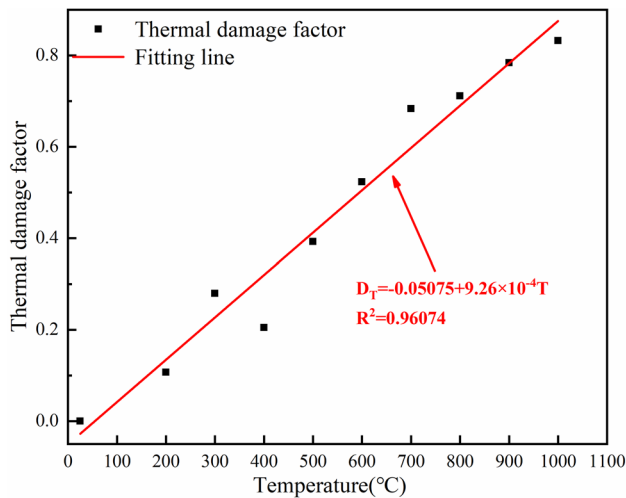


Fig. 11 Variation of the thermal damage factor with temperature

### 3.3.2 Compressive Damage Degree

Since the evolution of the rock micro-defect system is random, it can be regarded as an unbalanced statistical process. The intensity distribution of the micro-elements is believed to follow a Weibull distribution. Zhang et al. (2014) deduced a model of damage to rock subjected to heat and loading based on a Weibull distribution. The evolution in damage under uniaxial stress is described by Eq. (5). When the rock reaches failure, the geometric condition  $\epsilon_1 = \epsilon_f$  is satisfied. Therefore, Eq. (5) can be simplified as Eq. (6). The mechanical elastic modulus is calculated by Eq. (7).

$$D_m = 1 - \frac{E_{\tau T}}{E_{\tau 0}} \exp \left[ -\frac{1}{m} \left( \frac{\epsilon_1}{\epsilon_f} \right)^m \right] \tag{5}$$

$$D_m = 1 - \frac{E_{\tau T}}{E_{\tau 0}} \tag{6}$$

$$E_{\tau} = \frac{\Delta\sigma}{\Delta\epsilon} \tag{7}$$

where  $E_{\tau}$  is the elastic modulus calculated from the stress–strain curve;  $\Delta\sigma$  is the longitudinal stress increment in the straight-line segment of the stress–strain curves;  $\Delta\epsilon$  is the strain increment in the straight-line segment of the stress–strain curves;  $D_m$  is the compressive damage factor;  $E_{\tau T}$  and  $E_{\tau 0}$  are the mechanical elastic moduli at temperature  $T$  and room temperature, respectively;  $\epsilon_f$  is the peak strain;  $\epsilon_1$  is the strain in the direction of the first principal stress; and  $m$  is the Weibull parameter.

Figure 12 shows the relationship between temperature and the comprehensive damage factor of sandstone, as calculated by Eq. (6). The comprehensive damage factor reflects

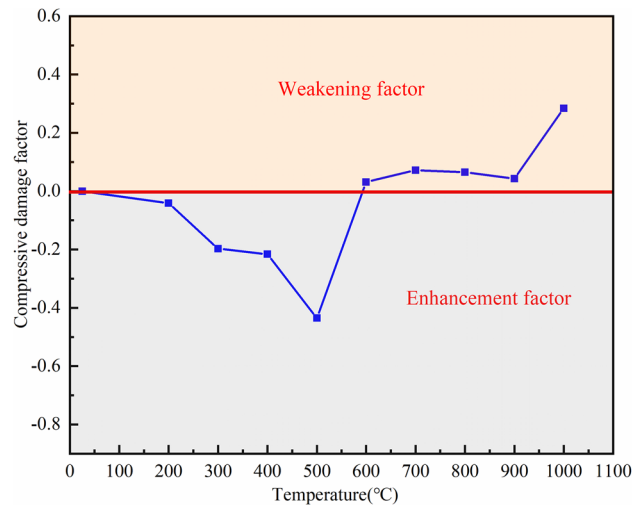


Fig. 12 Variation of the compressive damage factor with temperature

the damage degree under the influence of temperature and uniaxial load. When the result of Eq. (6) is negative, it indicates that the mechanical properties of sandstone are enhanced; conversely, the sandstone is weakened when the result is positive. It can be seen from Fig. 12 that changes in the comprehensive damage factor in response to temperature and load can be roughly divided into two stages. Below 500 °C, the factor is negative and the mechanical properties of sandstone are enhanced, with the mechanical strength reaching a maximum at 500 °C. The calculated damage factor is positive above 500 °C, indicating that the mechanical properties of sandstone become degraded under the actions of temperature and load. The damage factor changes greatly between 500 °C and 600 °C, meaning that the mechanical strength deteriorates rapidly due to the phase transition of quartz. The relationship between the comprehensive damage factor and temperature corresponds well with that of uniaxial compressive strength with temperature.

### 3.3.3 Dynamic Damage Degree During the Loading Process

The failure of rock under load is a progressive process. To quantitatively describe the dynamic failure process of rocks from deformation to macroscopic failure, it is necessary to describe the failure process in terms of damage variables. AE technology monitors rock crack evolution in essence; therefore, it is feasible to calculate the dynamic damage degree of rock based on AE cumulative ringing counts. The specific formula for the dynamic damage factor is as follows (Kong et al. 2019):

$$D_D = \left( 1 - \frac{\sigma c}{\sigma p} \right) \frac{\Omega}{\Omega m} \tag{8}$$

where  $D_D$  is the dynamic damage factor,  $\Omega$  is the cumulative ringing count of each stage,  $\Omega_m$  is the cumulative ringing count of the entire failure process,  $\sigma_c$  is the residual strength, and  $\sigma_p$  is the peak strength.

Taking the failure process of the sandstone sample at 1000 °C as an example, it can be seen from Fig. 13 that the dynamic damage evolution process of the rock has good correspondence with the stress and deformation development process. The dynamic damage factor hardly changes in the initial stage of loading, indicating that the external force does not cause much damage to the rock. As the stress increases further, the dynamic damage factor increases greatly and the growth rate also increases continuously, which means that the cracks inside the rock have entered the stage of unstable development. The damage factor decreases rapidly after rock failure. Dynamic damage factor characterization can be analyzed in conjunction with the AE results to better reveal and quantitatively describe the damage degree at different stages of the rock failure process.

### 3.4 Microscopic Analysis

#### 3.4.1 Results of SEM Analysis

Figure 14 shows SEM images of the crack structures developed inside the sandstone at different temperatures after failure. The sandstone used in this experiment was a sedimentary rock in its natural state with a certain number of pre-existing fissures and pores, as shown in Fig. 14(a). These defects affect the properties of sandstone. As the temperature increased from 25 °C to 500 °C, the number and size of cracks were almost unchanged. The quartz grains inside the sandstone closed to a certain extent due to thermal stress, which led to improvements in uniaxial compressive strength (Fig. 5). At the same time, the sandstone contained intergranular cracks along the quartz grain boundaries,

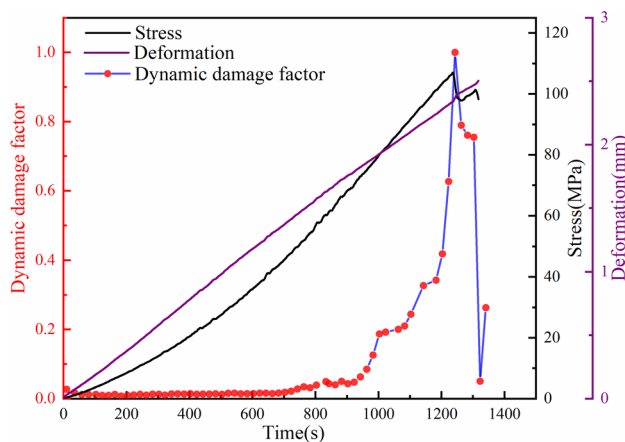


Fig. 13 Damage evolution in the whole process of loading (1000 °C)

transgranular cracks inside the quartz grains, and a small amount of exfoliated quartz grains separated from the surface within this temperature range. When the temperature reached 600 °C, the quartz inside the sandstone suffered phase transition (Xi et al. 1994; Deng et al., 2020), resulting in a greater degree of opening among the cracks than at room temperature. After 600 °C, the number and size of cracks in the sandstone increased, among which the number of transgranular cracks changed significantly. At ultra-high temperatures (> 600 °C), there is uncoordinated deformation among mineral particles due to their different thermal expansion coefficients, and the sandstone experiences mineral phase transition and sintering. Under the combined action of these factors, the original cracks continuously expand, extend and connect with each other, and new cracks are constantly generated and expanded, which leads to serious damage to the whole sample.

In summary, the distribution of cracks is random and is mainly related to the thermal and mechanical properties of the mineral components and their sizes and shapes. For example, cracks are mostly distributed in the short-axis direction of the mineral particles, at the dominant crystal surfaces, at the singular particle interfaces, and at other positions. At different temperature stages, the factors controlling the crack distribution also differ. Below 500 °C, the factors controlling crack development and distribution are mainly loss of water (such as free water, crystal water, structural water) and thermal expansion of mineral particles. Above 500 °C, the controlling factors are thermal expansion, mineral phase transition and mineral sintering (Su et al. 2008; Wu et al. 2007).

#### 3.4.2 Distribution of Cracks After Thermal Treatment

While SEM can be used to observe crack morphology in rock samples, it is difficult to distinguish the size and morphology of mineral particles and the type of mineral the crack is associated with. The microstructural damage induced by temperature has a great effect on the mechanical properties of rock, and the formation of micro-cracks increases the porosity. Figure 15 shows a microscopic image of the internal structure of sandstone treated at different temperatures. Micro-cracks are mainly caused by uncoordinated deformation among different mineral particles. At room temperature Fig. 15(a), it can be seen that some original cracks are distributed between quartz grains, muscovite grains and a small amount of kaolinite (a weathering product of feldspar) distributed between the quartz grains. The SEM images show that at 200 °C and 500 °C, intergranular cracks appear in the internal structure between quartz grains and between quartz and muscovite grains, and there are thermally-induced transgranular cracks on quartz grains. The quartz suffers phase transition at 600 °C, resulting in

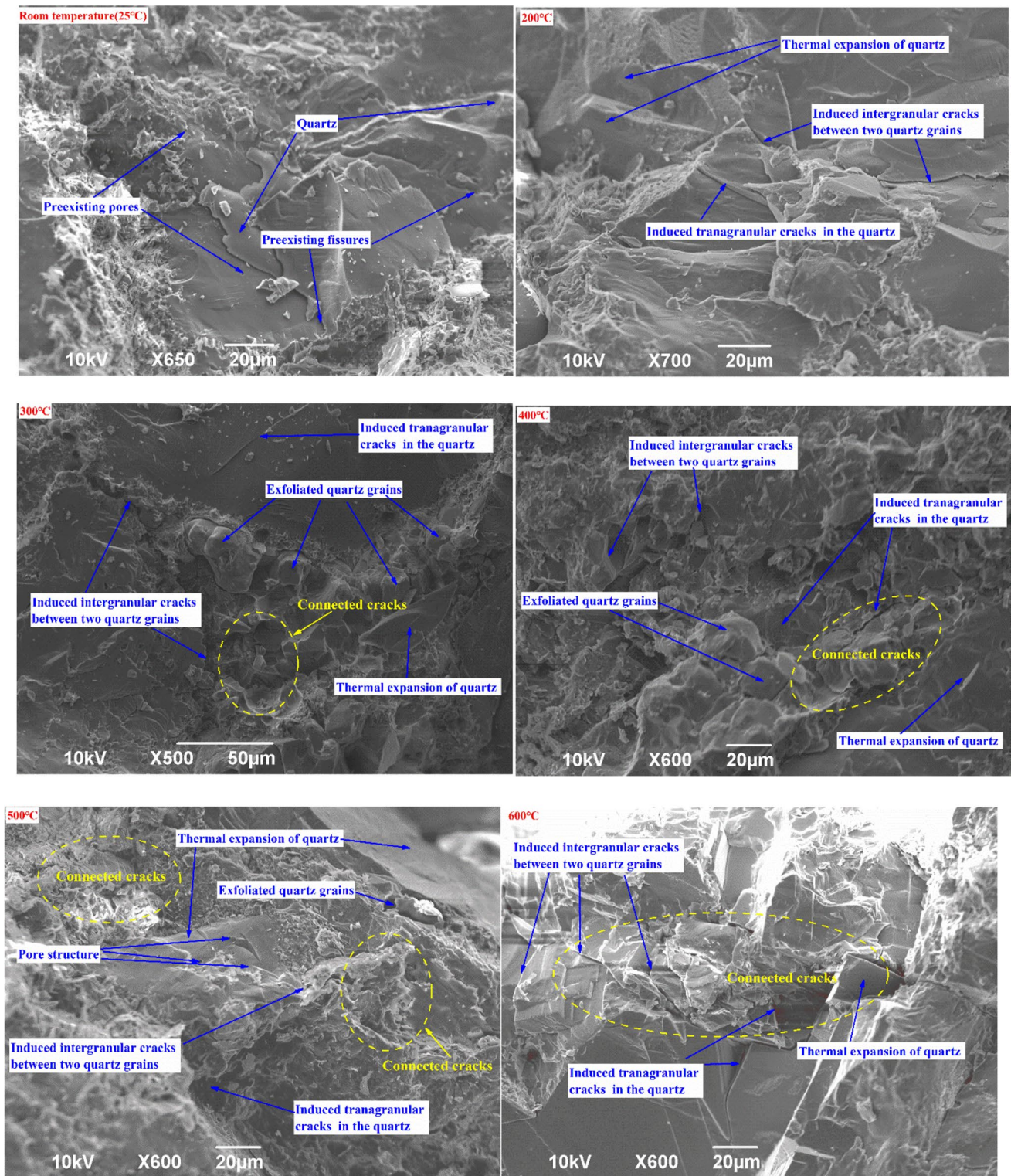


Fig. 14 Micro-structure of sandstone after heat treatment

cracks opening to a larger degree. At 700 °C and 900 °C, the size and number of cracks formed inside quartz grains and at the boundaries of quartz grains become larger, and

the integrity of the internal structure was reduced. The sandstone suffers serious and irreversible damage after thermal treatment, leading to decreases in parameters such as peak

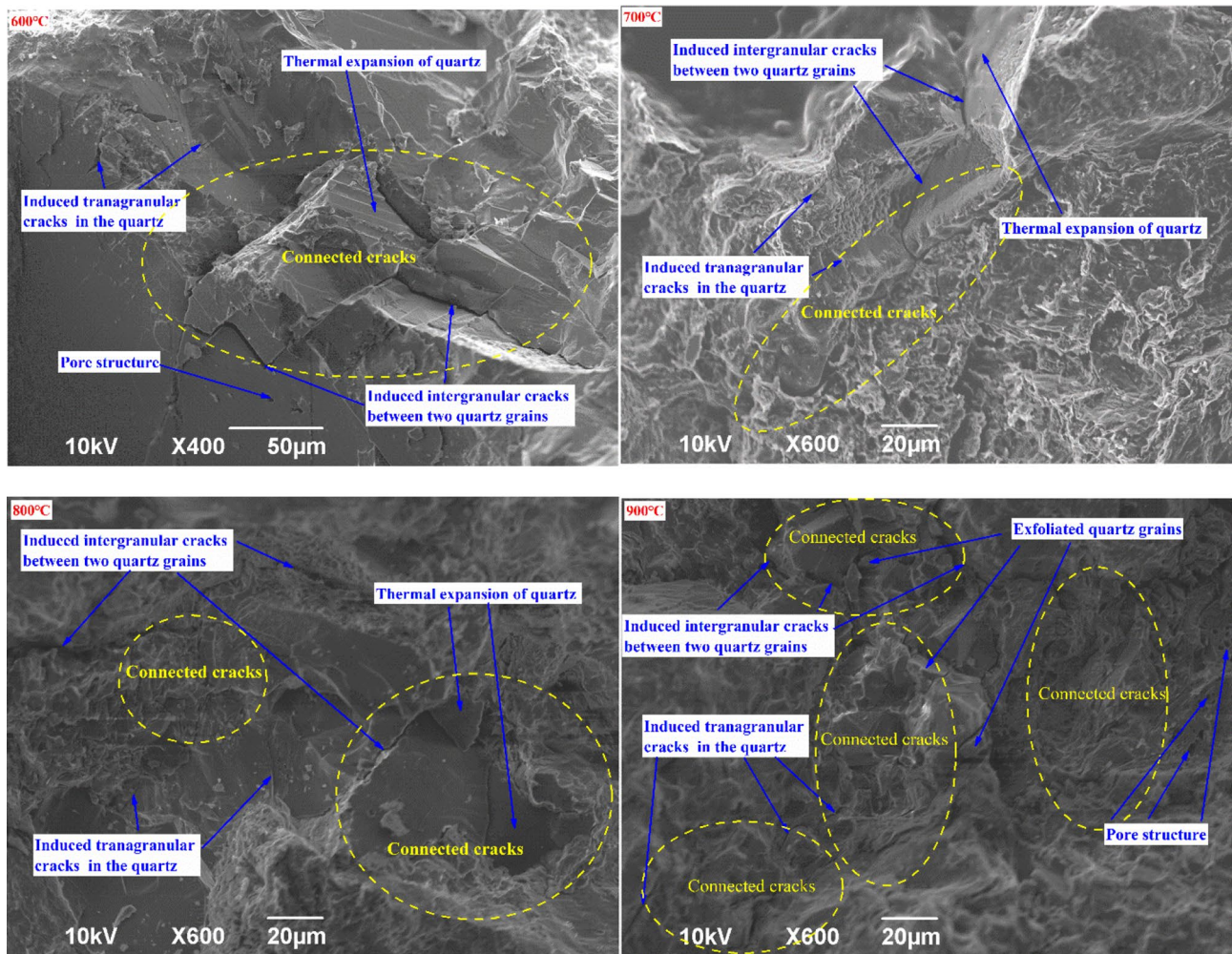


Fig. 14 (continued)

stress (Fig. 5). From the microscopic analysis of sandstone sections, it can be concluded that damage is gradually aggravated by increases in temperature, which is consistent with the analysis of Fig. 11.

### 3.4.3 Relationship Between Grain Size and UCS

Rock has variable heterogeneity, porosity, grain-size distributions and shapes, which affect its physical and mechanical properties (Ju et al. 2008). It is worth accurately describing the grain-size distribution and pore characteristics of rock to establish relationships with its physical and mechanical properties. The grain size was estimated from the thin-section microscope images in Fig. 15. The grain size is influenced by the difference between the samples themselves and by heating treatment. For example, thermally-induced micro-cracks divide the mineral particles, causing a change in particle size. The ratio of grain length ( $L$ ) to width ( $W$ )

was used to determine a grain size factor  $\alpha$ , as follows (Ding et al. 2020):

$$\alpha = \frac{L}{W} \quad (9)$$

Figure 16(a) depicts the relationship between the average grain size factor of sandstone and its compressive strength at different temperatures, it shows that there is good correspondence between the trends in grain size factor and uniaxial compressive strength, which are almost opposite, representing a reciprocal relationship; the smaller the grain size, the greater the uniaxial compressive strength. In the 500 °C–600 °C range, the size of sandstone grains decreases significantly, suggesting that cracks induced by temperature reduce grain sizes; for example, transgranular cracks may split mineral particles.

The uniformity of the rock mineral grain-size distribution also affects the physical and mechanical properties of rock. This can be characterized by the standard deviation of grain

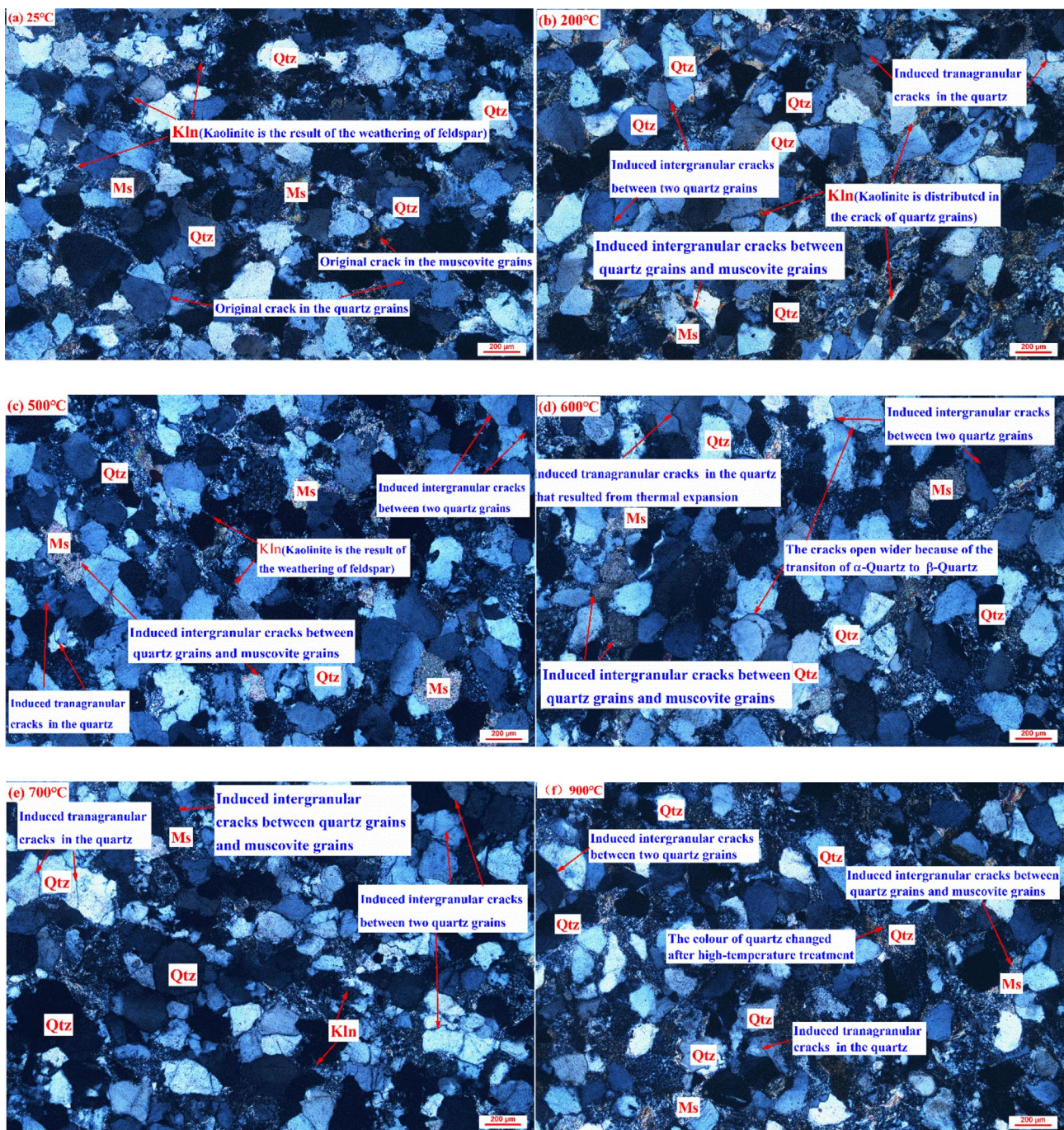


Fig. 15 Polarizing microscope images of sandstone after thermal treatment

size. The more uneven the size distribution, the better the sandstone grain gradation and the greater the mechanical strength. Figure 16(b) shows the variation in the standard deviation of mineral grain size with temperature in sandstone, showing that the trends in the two changes are similar. The standard deviation of grain size is the maximum at 500 °C, indicating that the grain size distribution is not uniform at this temperature. This also means that the grain size is

well graded and the pores between mineral particles will be few, so that the uniaxial compressive strength of sandstone is greatest at 500 °C.

### 3.5 XRD Analysis

The mineral composition of the rock is an important factor affecting its physical and mechanical properties (Zhang

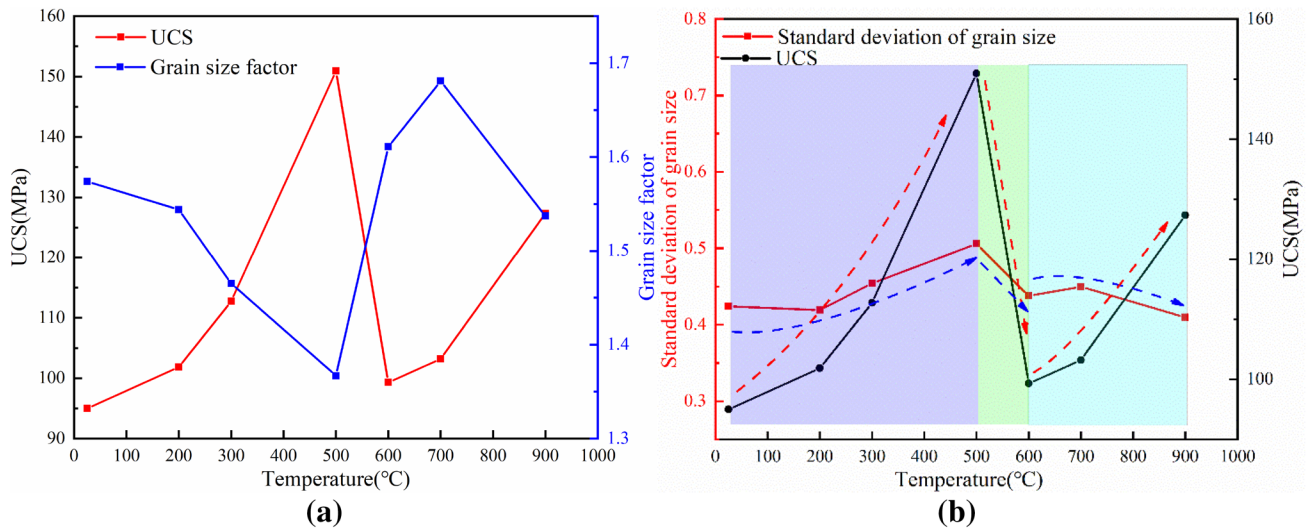
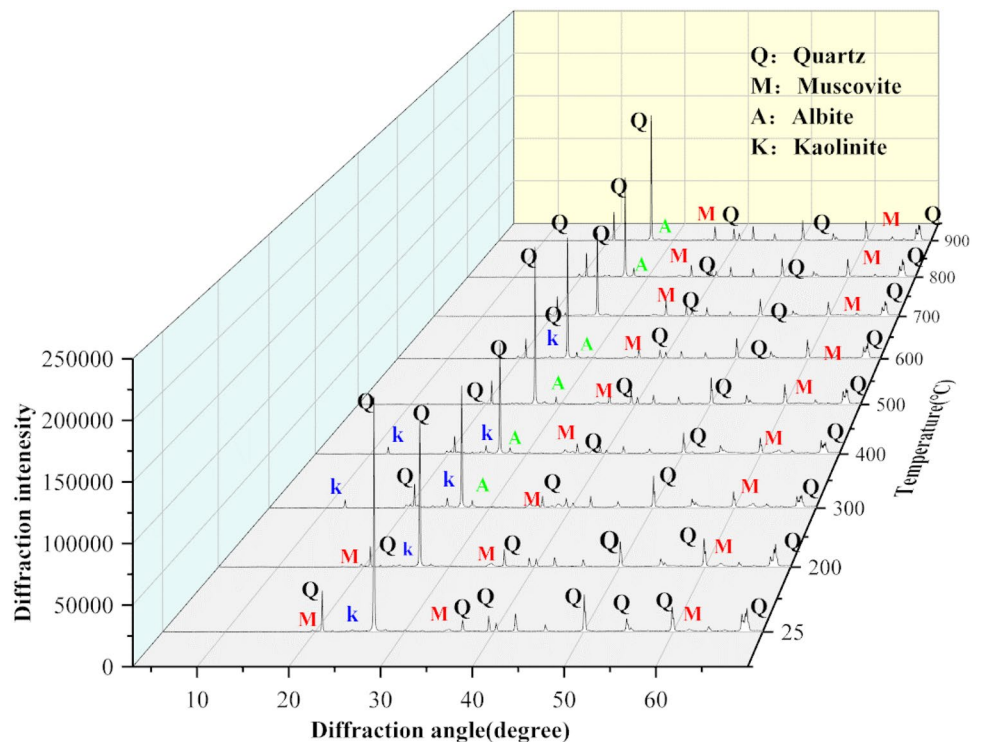


**Fig. 16** Effect of grain size on the UCS after thermal treatment. **(a)** Grain size factor; **(b)** Standard deviation of grain size

et al. 2020b). Any physical or chemical reaction in rock essentially changes its mineral composition. Figure 17 shows XRD patterns of the rock at different temperatures. According to these patterns, the minerals in the sandstone are mainly quartz with small amounts of muscovite, feldspar and kaolinite. Analysis of the diffraction peaks at different temperatures shows that there is no obvious change; however, the quartz changed after heat treatment. This can

be determined from the changes in diffraction intensity and diffraction angle in the XRD spectra. For example, the maximum diffraction intensity of the quartz changes at a different temperature, the maximum diffraction intensity of the quartz is 196632 at room temperature, and the lowest is 90257 at 700 °C, which is about 46% of that at room temperature. In addition, some trace minerals have different diffraction angle at different temperatures. Kaolinite has

**Fig. 17** XRD patterns of sandstone rocks at different temperatures

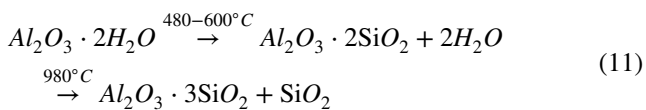
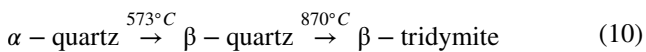




diffraction intensity peaks of 7945 and 6848 at the diffraction angle of  $12.2^\circ$  at  $300^\circ\text{C}$  and  $400^\circ\text{C}$ , respectively, but not at other temperatures. Quartz is the most abundant mineral in sandstone, so changes in quartz properties will greatly affect the physical and mechanical properties of the rock. For example, a transition from  $\alpha$ -quartz to  $\beta$ -quartz occurs at  $573^\circ\text{C}$  and a transition from  $\beta$ -quartz to  $\beta$ -tridymite occurs at  $870^\circ\text{C}$  (as shown in Eq. 10; Xi et al. 1994). Phase transition of quartz is accompanied by volumetric expansion, which increases cracking. Meanwhile, quartz phase transition transforms the quartz structure and physical properties, which greatly affect the physical and mechanical properties of the rock. This was fully demonstrated in the previous analysis.

Kaolinite also reacts at high temperature, further affecting the physical and mechanical properties of sandstone. For example, kaolinite changes to a metakaolinite phase at temperatures of  $480^\circ\text{C}$ – $600^\circ\text{C}$  and, at about  $980^\circ\text{C}$ , metakaolinite transforms to Al-Si spinels and decomposes  $\text{SiO}_2$  at the same time. This sequence of reactions is shown by Eq. 11 (Wang et al. 2010).

At  $800^\circ\text{C}$ – $900^\circ\text{C}$ , muscovite removes a large number of hydroxyl groups in the mineral structure and the mineral characteristics change greatly, which further weakens the physical and mechanical properties of sandstone (Liu 2009).



### 3.6 Comparison With Existing Literature

The most direct impacts of thermal damage are changes to the physical and mechanical properties of rock, such as its uniaxial compressive strength, tensile strength, elastic modulus, Poisson's ratio, mass, thermal expansion and P-wave velocity. Thermodynamic properties differ due to the different types and structures of the sandstone. Changes in the normalized peak strain and normalized uniaxial compressive strength of the sandstone under different heat-treatment conditions as reported by existing studies are summarized in Fig. 18. As can be seen in Fig. 18(a), the uniaxial compressive strengths of different types of sandstones show fluctuating changes after heat treatment. The studies by Wu et al. (2017), Ping et al. (2019) and Wang et al. (2013) showed an overall increase in uniaxial compressive strength before  $500^\circ\text{C}$ , which is similar to the results of this paper. After  $500^\circ\text{C}$ , the

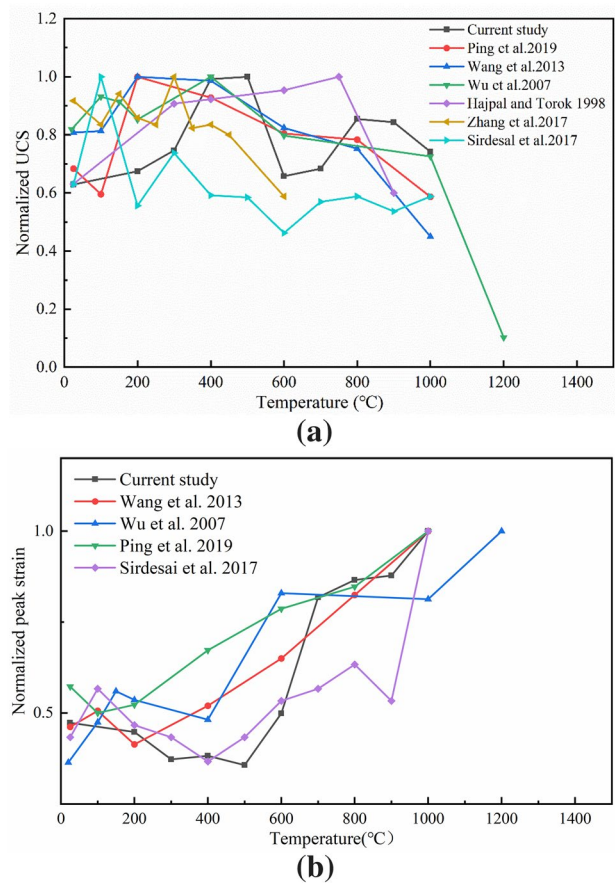


**Fig. 18** Comparisons with existing literature. **a** Variation of the normalized UCS with temperature; **b** Variation of normalized peak strain with temperature

uniaxial compressive strength of the sandstone is generally decreasing. Analysis of the normalized peak strains in Fig. 18(b) shows that the results of this paper are similar to those of other literature in that the peak strains are increasing. The variability in the strength and deformation characteristics of different types of sandstones is mainly related to the internal structure and mineral fraction, which is the key and difficulty of this paper.

## 4 Conclusions

The physical and mechanical properties of rock change greatly after heating, mainly due to changes in mineral composition and microstructure. In this paper, the physical and mechanical properties of sandstone treated at a range of temperatures ( $25^\circ\text{C}$ – $1000^\circ\text{C}$ ) were analysed. The essence of thermal damage was further revealed by AE monitoring, SEM, polarized light microscopy and XRD.

- (1) It was found that the mechanical parameters of the sandstone, such as average uniaxial compressive strength and peak strain generally show trends of improvement at about 25–500 °C and then weaken at 600 °C–1000 °C. The opening degree of crack decreases at the low temperature observed from SEM images, resulting in improved mechanical properties. At high temperatures, cracks interconnect with each other, which degrades the mechanical properties of the sandstone. The damage mode in the sandstone is mostly shear failure, with the higher the temperature the more severe the damage.
- (2) AE signals become more active with increasing temperature. Parameters such as AE hits, AE events, AE energy and AE counts all increase with temperature. The analysis of the AE b-values indicate that small cracks are predominantly produced within the rock during the initial loading stage and that large-scale cracks develop during the later loading stage. The study shows that the static and dynamic damage degree to the sandstone becomes increasingly serious with increases in temperature and external force by defining three damage variables including thermal damage variables, compressive damage variables and dynamic damage variables.
- (3) The mineral composition of the sandstone does not change significantly with increasing temperature according to XRD; however, physical and chemical reactions in quartz, muscovite and kaolinite at high temperatures seriously affect the physical and mechanical properties of the sandstone. It also draws that the crack distribution is the fundamental cause of thermal damage based on polarized light microscopy. Grain size and pore distribution also affect the uniaxial compressive strength of the rock, with larger grains with a less even distribution being associated with better mechanical properties in the sandstone.

**Acknowledgements** This research is supported by the Innovative and creative research program for doctoral students of Nanjing University (XCXY-19-62), the financial support from the National Natural Science Foundation of China (41702326), the Innovative Experts, Long-term Program of Jiangxi Province (jxsq2018106049), 2018 Qing Lan Project of Jiangsu Province, and the Supported by Program of Qingjiang Excellent Young Talents, Jiangxi University of Science and Technology.

**Author Contributions** LCD, XZL, YCW, YW, ZH and CLJ conceptualized the study. LCD and XZL conducted the data acquisition, preparation, and analysis. All authors contributed to the interpretation of results and manuscript preparation.

**Data Availability** All data used in this study are true and reliable, it can be freely available through open data portals online.

## Declarations

**Conflict of interest** The authors declare that they have no known competing financial interests or personal relationships that could have appeared to influence the work reported in this paper.

## References

- Cai M, Kaiser PK, Tasaka Y, Maejima T, Morioka H, Minami M (2004) Generalized crack initiation and crack damage stress thresholds of brittle rock masses near underground excavations. *Int J Rock Mech Min Sci* 41:833–847
- Deng LC, Li XZ, Wu Y, Xu ZH, Huang Z, Jiang CL, Yuan DM (2020) Study on mechanical damage characteristics of granite with different cooling methods. *J China Coal Soc.* <https://doi.org/10.13225/j.cnki.jccs.2020.1284>
- Ding QL, Ju F, Song SB, Yu BY, Ma D (2016) An experimental study of fractured sandstone permeability after high-temperature treatment under different confining pressures. *J Nat Gas Sci Eng* 34:55–63
- Ding ZW, Li XF, Tang QB, Jia JD (2020) Study on correlation between fractal characteristics of pore distribution and strength of sandstone particles. *Chin J Rock Mech Eng* 39:1–9
- Dorn RI (2003) Boulder weathering and erosion associated with a wildfire, Sierra Ancha Mountains, Arizona. *Geomorphology* 55:155–171
- Fairhurst C, Hudson J (1999) Draft ISRM suggested method for the complete stress-strain curve for intact rock in uniaxial compression. *Int J Rock Mech Min Sci* 36(3):279–289
- Feng G, Kang Y, Chen F, Liu YW, Wang XC (2018) The influence of temperatures on mixed-mode (I + II) and mode-II fracture toughness of sandstone. *Eng Fract Mech* 189:51–63
- Feng G, Wang XC, Wang M, Kang Y (2020) Experimental investigation of thermal cycling effect on fracture characteristics of granite in a geothermal-energy reservoir. *Eng Fract Mech* 235:107180
- Ferrero AM, Migliazza M (2009) Theoretical modelling of bowing in cracked marble slabs under cyclic thermal loading. *Constr Build Mater* 23(6):2151–2159
- Fitzner B, Heinrichs K, Bouchardiere LD (2003) Weathering damage on pharaonic sandstone monuments in Luxor-Egypt. *Build Environ* 38:1089–1103
- Fu B, Zhou ZH, Wang HQ, Wang YX (2016) Precursor information study on acoustic emission characteristics of marble under uniaxial cyclic loading-unloading. *J China Coal Soc* 41(8):1946–1953
- Fuenkajorn K, Sriapai T, Samsri P (2012) Effects of loading rate on strength and deformability of Maha Sarakham salt. *Eng Geol* 135–136:10–23
- Gautam PK, Verma AK, Jha MK, Sarkar K, Singh TN, Bajpai RK (2016a) Study of strain rate and thermal damage of dholpur sandstone at Elevated Temperature. *Rock Mech Rock Eng* 49:3805–3815
- Gautam PK, Verma AK, Maheshwar S, Singh TN (2016b) Thermo-mechanical analysis of different types of sandstone at elevated temperature. *Rock Mech Rock Eng* 49:1985–1993
- Gutenberg B, Richter CF (1944) Frequency of earthquakes in California. *Bull Seismol Soc Am* 34(4):185–188
- Hajpal M (2002) Changes in sandstones of historical monuments exposed to fire or high temperature. *Fire Technol* 38:373–382
- Hajpal M, Torok A (1998) Petrophysical and mineralogical studies of burnt sandstones. In: 2nd International PhD Symposium in Civil Engineering. Budapest, Hungary, pp, 1–9
- Han GS, Jing HW, Su HJ, Yin Q, Wu JY, Gao Y (2020) Experimental research on mechanical behaviors of water-cooled sandstone

- after high temperature treatment. *J China Univ Mining Technol* 49(1):70–75
- Huang Z, Zeng W, Wu Y, Li SJ, Gu QX, Zhao K (2021a) Effects of temperature and acid solution on the physical and tensile mechanical properties of red sandstones. *Environ Sci Poll Res* 28:20608–20623
- Huang Z, Zeng W, Gu Q, Wu Y, Zhong W, Zhao K (2021b) Investigations of variations in physical and mechanical properties of granite, sandstone, and marble after temperature and acid solution treatments. *Constr Build Mater* 307(8):124943
- Ju Y, Yang YG, Song ZD, Xu WJ (2008) Statistical model of rock pore structure. *Sci Sinica (technologica)* 7:1026–1041
- Kong B, Wang EY, Li ZH, Wang XR, Liu XF, Li N, Yang YL (2016) Electromagnetic radiation characteristics and mechanical properties of deformed and fractured sandstone after high temperature treatment. *Eng Geol* 209:82–92
- Kong B, Wang EY, Li ZH, Wang XR, Niu Y, Kong XG (2017) Acoustic emission signals frequency-amplitude characteristics of sandstone after thermal treated under uniaxial compression. *J Appl Geophys* 136:190–197
- Kong XG, Wang EY, Wang SG, Lin HF, Zhang JZ (2019) Fractals and chaos characteristics of acoustic emission energy about gas-bearing coal during loaded failure. *Fractals* 27(5):1–11
- Li LM, Lei RD (2020b) Experimental study on mechanical properties and AE of thermally damaged sandstone. *Safety Coal Mines* 51(5):72–77
- Li C, Hu YQ, Zhang CW, Zhao ZR, Jing PH, Hu YF, Zhao GK (2020b) Brazilian split characteristics and mechanical properties evolution of granite after cyclic cooling at different temperatures. *Chin J Rock Mech Eng* 39:1–11
- Li M, Wang DM, Shao ZL (2020a) Experimental study on changes of pore structure and mechanical properties of sandstone after high-temperature treatment using nuclear magnetic resonance. *Eng Geol* 275:105739. <https://doi.org/10.1016/j.enggeo.2020.105739>
- Liu C (2010) Change of structure of micro-crystalline muscovite in the course of high temperatures and its impact on dielectric properties. Chengdu University of Technology
- Liu QS, Xu XC (2000) Damage analysis of brittle rock at high temperature. *Chin J Rock Mech Eng* 19(4):408–411
- Liu XL, Pan MC, Li XB, Wang JP (2017) Acoustic emission b-value characteristics of granite under dynamic loading and static loading. *Chinese J Rock Mech Eng* 36(sup1):3148–3155
- Liu XL, Liu Z, Li XB, Han MS (2019) Acoustic emission b-values of limestone under uniaxial compression and Brazilian splitting loads. *Rock Soil Mech* 40(sup1):267–274
- Liu Z, Yao QG, Kong B, Yin JL (2020) Macro-micro mechanical properties of building sandstone under different thermal damage conditions and thermal stability evaluation using acoustic emission technology. *Construct Build Mater* 246:118485
- Lu C, Sun Q, Zhang WQ, Geng JS, Qi YM, Lu LL (2017) The effect of high temperature on tensile strength of sandstone. *Appl Therm Eng* 111:573–579
- Mahanta B, Vishal V, Ranjith PG, Singh TN (2020) An insight into pore-network models of high-temperature heat-treated sandstones using computed tomography. *J Nat Gas Sci Eng* 77:103227
- Malkowski P, Kaminski P, Krzysztof S (2012) Impact of Heating of carboniferous rocks on their mechanical parameters. *AGH J Mining Geology* 36(1):231–242
- Nara Y, Morimoto K, Yoneda T, Hiroyoshi N, Kaneko K (2011) Effects of humidity and temperature on subcritical crack growth in sandstone. *Int J Solids Struct* 48:1130–1140
- Ping Q, Wu MJ, Zhang H, Yuan P (2019) Experimental study on dynamic mechanical characteristics of sandstone under actual high temperature conditions. *Chinese J Undergr Space Eng* 15:691–697
- Rong HR, Wang HL, Fang JH, Cao HY, Wang ZS, Wang DL, Dong H (2018) Experimental study of influence of fire temperature change on sandstone structure of tunnel. *Indian Safety Environ Prot* 44(08):4–8
- Shen YJ, Wang YZ, Zhao XD, Yang GS, Jia HL, Rong TL (2018) The influence of temperature and moisture content on sandstone thermal conductivity from a case using the artificial ground freezing (AGF) method. *Cold Reg Sci Technol* 155:149–160
- Sirdesai N, Singh TN, Pathegama Gamage R (2017) Thermal alterations in the poro-mechanical characteristic of an Indian sandstone – a comparative study. *Eng Geol* 226:208–220
- Sirdesai NN, Gupta T, Singh TN, Ranjith PG (2018) Studying the acoustic emission response of an Indian monumental sandstone under varying temperatures and strains. *Constr Build Mater* 168:346–361
- Su CD, Guo WB, Li XS (2008) Experimental research of mechanical properties of coarse sandstone after high temperatures. *Chinese J Rock Mech Eng* 27(6):1162–1170
- Su HJ, Jing HW, Zhao HH, Yi Q (2015) Study on tensile strength and size effect of red sandstone after high temperature treatment. *Chinese J Rock Mech Eng* 34(sup1):2879–2887
- Sun Q, Lu C, Cao LW, Li WC, Geng JS, Zhang WQ (2016) Thermal properties of sandstone after treatment at high temperature. *Int J Rock Mech Min Sci* 85:60–66
- Sun H, Sun Q, Deng WN, Zhang WQ, Lu C (2017) Temperature effect on microstructure and P-wave propagation in Linyi sandstone. *Appl Therm Eng* 115:913–922
- Tian H, Kempka T, Yu S, Ziegler M (2016) Mechanical properties of sandstones exposed to high temperature. *Rock Mech Rock Eng* 49:321–327
- Verma AK, Saini MS, Singh TN, Dutt A, Bajpai RK (2013) Effect of excavation stages on stress and pore pressure changes for an underground nuclear repository. *Arab J Geosci* 6(3):635–645
- Wang CS, Shao S, Zhou ZG, Long F, Yi MZ (2010) High temperature carbothermal reaction mechanism of kaolinite/carbon system. *Mater Sci Eng Powder Meta* 15(4):317–323
- Wang P, Xu JY, Liu JY, Cheng TF (2013) Research on dynamic mechanical properties of sandstone at high temperature. *ACTA Rmamentarii* 34:203–208
- Wang P, Xu JY, Fang XY, Wen M, Zheng GH, Wang PX (2017) Dynamic splitting tensile behaviors of red-sandstone subjected to repeated thermal shocks: deterioration and micro-mechanism. *Eng Geol* 223:1–10
- Wu Z, Qin BD, Chen LJ, Luo YJ (2005) Experimental study on mechanical character of sandstone of the upper plank of coal bed under high temperature. *Chin J Rock Mech Eng* 24(11):1863–1867
- Wu G, Xing AG, Zhang L (2007) Mechanical characteristics of sandstone after high temperatures. *Chin J Rock Mech Eng* 26(10):2110–2116
- Wu SC, Guo P, Zhang SH, Zhang G, Jiang RH (2018) Study on thermal damage of granite based on Brazilian splitting test. *Chinese J Rock Mech Eng* 37(sup2):3805–3815
- Wu Y, Huang Z, Zhao K, Zeng W, Gu QX, Zhang R (2020) Unsteady seepage solutions for hydraulic fracturing around vertical-wellbores in hydrocarbon reservoirs. *Int J Hydrog Energy* 45(16):9496–9503
- Wu Y, Li XZ, Huang Z, Xue S (2021) Effect of temperature on physical, mechanical and acoustic emission of Beishan granite. *Nat Hazards* 107:1577–1592
- Xi DY (1994) The physical characteristics of mineralogical variation in granite. *Acta Mineral Sinica* 14(3):223–227
- Yang SQ, Jing HW, Huang YH, Ranjith PG, Jiao YY (2014) Fracture mechanical behavior of red sandstone containing a single fissure and two parallel fissures after exposure to different high temperature treatments. *J Struct Geol* 69:245–264
- Yang SQ, Xu P, Li YB, Huang YH (2017) Experimental investigation on triaxial mechanical and permeability behavior of sandstone

- after exposure to different high temperature treatments. *Geothermics* 69:93–109
- Yavuz H, Demirdag S, Caran S (2010) Thermal effect on the physical properties of carbonate rocks. *Internat J Rock Mech Mining Sci* 47:94–103
- Yin TB, Bai L, Li X, Li XB, Zhang SS (2018) Effect of thermal treatment on the mode I fracture toughness of granite under dynamic and static coupling load. *Eng Fract Mech* 199:143–158
- Yu J, Chen S, Chen X, Zhang Y, Cai Y (2015) Experimental investigation on mechanical properties and permeability evolution of red sandstone after heat treatments. *J Zhej Univ Sci A* 16:749–759
- Zeng YJ, Rong G, Peng J, Sha S (2018) Experimental study of crack propagation of marble after high temperature cycling. *Rock Soil Mech* 39(sup1):220–225
- Zhang WQ, Lv C (2020) Effects of mineral content on limestone properties with exposure to ferent temperatures. *J Petrol Sci Eng* 188:106941
- Zhang LY, Mao XB (2010) Experimental study of the mechanical effects of loading rates on limestone at high temperature. *Rock Soil Mechanics* 31(11):3511–3515
- Zhang HM, Lei LN, Yang GS (2014) Damage model of rock under temperature and load. *Chinese J Rock Mech Eng* 33(sup2):3391–3396
- Zhang YL, Sun Q, He H, Cao LW, Zhang WQ, Wang B (2017c) Pore characteristics and mechanical properties of sandstone under the influence of temperature. *Appl Therm Eng* 113:537–543
- Zhang R, Ai T, Gao MZ, Zhang GQ, Zhou C (2017b) Acoustic emission of rocks- Basic theory and experimental research. Sichuan University Press, pp 1–10
- Zhang Y, Sun Q, He H et al (2017c) Pore characteristics and mechanical properties of sandstone under the influence of temperature. *Appl Therm Eng* 113:537–543
- Zhang DM, Yang YS, Yang H, Yang S (2018) Experimental study on the effect of high temperature on the mechanical properties and acoustic emission characteristics of gritstone. *Res Phys* 9:1609–1617
- Zhang H, Sun Q, Liu L, Ge ZL (2020) Changes in glossiness, electrical properties and hardness of red sandstone after thermal treatment. *J Appl Geophys* 175:1–7
- Zhang JY, Shen YJ, Yang GS, Zhang H, Wang YZ, Hou X, Sun Q, Li GY (2021) Inconsistency of changes in uniaxial compressive strength and P-wave velocity of sandstone after temperature treatments. *J Rock Mech Geotech Eng* 13:143–153
- Zhao ZH, Dou ZH, Xu HR, Liu ZN (2019a) Shear behavior of Beishan granite fractures after thermal treatment. *Eng Fract Mech* 213:223–240
- Zhao PJ, Sun YD, Jiao JP, Fang G (2020) Correlation between acoustic emission detection and microstructural characterization for damage evolution. *Eng Fract Mech* 230:106941
- Zhao JJ, Fan Q, Li PF, Li SS, Wang G, Jie ML (2019b) Acoustic emission b-value characteristics and failure precursor of the dacite under different stress paths. *J Eng Geol* 27(3): 487–496
- Zhu TT, Jing HW, Su HJ, Yin Q, Du MR, Han GH (2016) Physical and mechanical properties of sandstone containing a single fissure after exposure to high temperatures. *Int J Min Sci Technol* 26:319–325
- Zhu ZN, Tian H, Dong NN, Dou B, Chen J, Zhang Y, Wang BH (2018) Experimental study of physical-mechanical properties of heat-treated granite by water cooling. *Rock Soil* 39(sup2):169–176

**Publisher's Note** Springer Nature remains neutral with regard to jurisdictional claims in published maps and institutional affiliations.